UNIVERSITY of York

This is a repository copy of *Asymmetries in the three-dimensional beat of Chlamydomonas reinhardtii flagella revealed by holographic microscopy*.

White Rose Research Online URL for this paper:
https://eprints.whiterose.ac.uk/id/eprint/230628/

Version: Accepted Version

Article:
Wilson, Laurence George orcid.org/0000-0001-6659-6001 and Bees, Martin Alan (2025) Asymmetries in the three-dimensional beat of Chlamydomonas reinhardtii flagella revealed by holographic microscopy. Journal of Cell Science. jcs263946. ISSN: 0021-9533

https://doi.org/10.1242/jcs.263946

Reuse
This article is distributed under the terms of the Creative Commons Attribution (CC BY) licence. This licence allows you to distribute, remix, tweak, and build upon the work, even commercially, as long as you credit the authors for the original work. More information and the full terms of the licence here: https://creativecommons.org/licenses/

Takedown
If you consider content in White Rose Research Online to be in breach of UK law, please notify us by emailing eprints@whiterose.ac.uk including the URL of the record and the reason for the withdrawal request.

White Rose university consortium
Universities of Leeds, Sheffield & York

eprints@whiterose.ac.uk
https://eprints.whiterose.ac.uk/

© 2025. Published by The Company of Biologists

Asymmetries in the three-dimensional beat of *Chlamydomonas reinhardtii* flagella revealed by holographic microscopy

Laurence G. Wilson[1] and Martin A. Bees[2]

[1]School of Physics, Engineering and Technology, University of York, Heslington, York, YO10 5DD, UK
[2]Department of Mathematics, University of York, Heslington, York, YO10 5DD, UK

Abstract

We present the first three-dimensional, time-resolved imaging of the *Chlamydomonas reinhardtii* flagellar waveform. This freshwater alga is a model system for eukaryotic flagella that allow cells to move and pump fluid. During the power stroke, the flagella show rotational symmetry about the cell's centre line, but during the recovery stroke they display mirror symmetry about the same axis. Furthermore, and in contrast to the usual assumptions about beat planarity, we show a subtle rotational motion of the flagella at the initiation of the power stroke, which is mechanically rectified into a quasi-planar mode. We apply resistive force theory to infer the swimming speed and rotational speed of the cells, when a force-free configuration is approximated using a cell on a micropipette, showing good agreement with experimental results on freely swimming cells.

Introduction

Symmetry and symmetry breaking are central concepts in physics that offer a powerful perspective on phenomena in the life sciences. An example is the eukaryotic flagellum, a highly conserved organelle (Khan and Scholey 2018) that allows cells to move and to pump fluid. Its central component, the axoneme, has a recognizable structural motif: a chiral arrangement of nine microtubule doublets encircling a central pair of singlets. Dynein motors cause the doublets to slide length-wise relative to each other, resulting in the whip-like motion for which the flagellum was named. Their early development in the eukaryotic lineage results in a wide range of roles throughout the domain: they propel sperm cells in groups as diverse as mammals and seaweed (Gaffney et al. 2011; Inouye and Hori 1991), and pump fluid in the human lung and brain (Kanale et

Journal of Cell Science • Accepted manuscript

al. 2022; Breunig et al. 2010). Moreover, cilia (we use the terms `flagella' and `cilia' interchangeably in our context) have been posited to play a role in symmetry breaking during embryonic development (Hirokawa et al. 2009), highlighting the delicate role of symmetry and symmetry breaking in their function.

The green alga *Chlamydomonas reinhardtii* is a unicellular model species for studying flagellar motility: it swims with a `breaststroke' motion, pulled by a pair of anterior flagella. Ultrastructural studies of *C. reinhardtii* flagella have observed the internal configuration of the axonemes and dynein motors with precision (Hoops and Witman 1983; Nicastro et al. 2006; Bui et al. 2012; Oda et al. 2014; Owa et al. 2019), and mutants without structures ensuring symmetry between flagella show degraded swimming ability (Hoops et al. 1984). Studying flagella in freely-swimming cells is challenging because *C. reinhardtii* swims in a helical trajectory at around 10 body lengths per second. To mitigate this, glass micropipettes have been used to hold individual cells (Hoops et al. 1984; Rüffer and Nultsch 1990; 1991; Polin et al. 2009), allowing a detailed study of flagellar dynamics. Flagella are challenging to image because of their small size (diameter typically less than 250 nm) and fast beating (10–100 Hz). Capturing their shape in three dimensions is essential to measuring chirality in their motion, and linking structure to function. Several groups have approached this problem, in various biological systems. Multi-plane phase contrast microscopy has been used to image isolated, reactivated *C. reinhardtii* flagella (Mojiri et al. 2021), and a more recent study using defocused dark field microscopy (Striegler et al. 2024) has given insight into the relationship between torsion and twist in isolated flagella. An exciting recent development is the application of `acoustofluidics' to confine cells to pressure nodes in a standing acoustic wave. This relatively soft confinement allows single cells or groups of cells to be localized in order to measure their rotational and flagellar beat dynamics (Cui et al. 2023). The flagellar kinematics of the singly-flagellated alga *Euglena* were extracted from phase contrast images using model-based fitting (Rossi et al. 2017), and the shape of beating tails of human sperm have been extracted from bright field microscopy images (Bukatin et al. 2015).

Imaging the three-dimensional flagellar beating of intact *C. reinhardtii* cells is challenging, as the cell body scatters a significant amount of light. To our knowledge, the first direct imaging of the out-of-plane component of these organelles was made by Rüffer and Nultsch, 35 years prior to our study (Rüffer and Nultsch 1985), who concluded that "[...] the movement of the flagellum is composed of two different components: the backward-forward movement and the smaller lateral clockwise-anticlockwise movement." Nevertheless, they ultimately attributed the helical swimming

Journal of Cell Science • Accepted manuscript

trajectories of these cells to asynchronous flagellar beating, a mechanism that seems unlikely in light of subsequent work (Polin et al. 2009). In an elegant study, Cortese and Wan (Cortese and Wan 2021) built a numerical model of three-sphere swimmer to explore *C. reinhardtii* navigation. They used `optical flow' image processing routines to estimate the extent of non-planarity in the flagellar beat from a two-dimensional projection of a cell. While this system works well in its aim of determining the angular extent of deviations from a planar beat, the relationship between changes in pixel intensity and flagellar position is not well defined for a weakly scattering object crossing the focal plane, and the resulting cardioidal shape of the tip trajectory does not, when projected on to two dimensions, match previous measurements (Rüffer and Nultsch 1985) or ours. This effect does not undermine the conclusions of that work, but future modelling efforts will require uncertainties in the positions of the beating flagella to be much reduced.

Our groups and others have successfully used digital holographic microscopy (DHM) (Kim 2010) to image *Plasmodium* microgametes (Wilson et al. 2013) and sperm flagella (Gong et al. 2021) in 3D. DHM is an ideal tool for expanding such studies: it is label-free, with localisation precision comparable to bright-field microscopy, and it is well suited to imaging weakly scattering microscopic objects (Wilson and Zhang 2012). A strong advantage of this method is the time resolution that it offers, which is limited only by the camera electronics. Using modern CMOS devices, imaging rates of hundreds to thousands of volumes per second are routine. DHM has been used to track swimming microorganisms including bacteria (Cheong et al. 2016; Molaei et al. 2014; Bianchi et al. 2017; Kühn et al. 2018; Gibson et al. 2021), archaea (Thornton et al. 2020), dinoflagellates (Sheng et al. 2007), sperm cells (Su et al. 2012; Jikeli et al. 2015; Gong et al. 2021), and other eukaryotes (Wilson et al. 2013; Findlay et al. 2021). Although the computational cost of the method has historically been a barrier to high-throughput usage, modern CPU/GPU architectures have made DHM accessible to anyone with a desktop computer, and artificial intelligence-based approaches accelerate the method to real-time processing (Hannel et al. 2018; Matthews et al. 2024). We use DHM to resolve the three-dimensional shape of the flagellar beat, and its temporal evolution, in wildtype (strain CC-125) and mutant (strain CC-2288, 'long flagella') *C. reinhardtii* cells.

Results

Time-averaged curvature and torsion

Fig. 1a shows an example of raw holographic data. After careful background subtraction, the dynamic parts of the image are revealed, as shown in Fig. 1b. These images were processed

Journal of Cell Science • Accepted manuscript

numerically using Rayleigh-Sommerfeld back propagation (Lee and Grier 2007) and a scheme based on the Gouy phase anomaly (Wilson and Zhang 2012) was used to localise the flagellar contour in three dimensions. We then analysed the shape of the flagella using the Frenet-Serret formulae to describe a three-dimensional curve in terms of unit tangent ($\hat{\mathbf{t}}$), normal ($\hat{\mathbf{n}}$) and binormal ($\hat{\mathbf{b}}$) vectors.

Figures 1c,d show the flagella during power and recovery strokes. Figures 1e,f show the cell- and time-averaged flagellar curvature (κ) and torsion (τ) for CC-125 cells (N=20 cells) and Figs.1g,h show the equivalent data for CC-2288 cells (N=16 cells). In both strains, the curvature and torsion are well resolved for low values of the contour length s, but become noisy at the distal ends of the flagella due to poor statistics (i.e. few cells have the longest flagella, and camera noise leads to occasional 'missed detections'). Both CC-125 and CC-2288 show modest average torsion, with zero average torsion lying within the 95% confidence intervals. However, it should be noted that for nearly-straight sections of the flagellum, $\kappa \to 0$ and we find large fluctuations in τ. We therefore restrict our discussion of τ to phases during which it is well-resolved (an examination of how position uncertainties affect the results is presented in the methods section and Fig. S1).

Orientations of power and recovery strokes

Figure. 2a,b,c shows the flagellar beat envelope, averaged over 500 cycles. Surface normal vectors of the planes traced out by power and recovery strokes are indicated by C_1, T_1 (power) and C_2, T_2 (recovery), where C and T indicate cis and trans flagella relative to the cells' eye spots. Without loss of generality, we set C_1 to point upwards in our coordinate system, and define the other vectors (C_2, T_1, T_2) from this. The angle between $C_1$and T_1 is around 30 degrees, in good agreement with previous work based on 2D projections (Cortese and Wan 2021). However, unlike previous studies, we find that a flagellum's power and recovery strokes lie in different planes. Figure 2d shows the angles between beat planes across both strains (CC-125 and CC-2288), consistent with the mutants having flagella that are slightly longer but otherwise similar to wildtype.

Chiral asymmetry in the flagellar beat

A kymograph of $\kappa(t)$ is shown in Fig. 3a,d. Light colored bands corresponding to high curvature propagate from the proximal to the distal ends of the flagella at speeds around 1 mm/s, and frequencies of 40–50 Hz. The waves of high curvature correspond to the recovery stroke, as the flagella move to the front of the cell. When examined in closer detail, intriguing differences emerge between the cis and trans flagellar waveforms during the power and recovery strokes. The recovery

Journal of Cell Science • Accepted manuscript

stroke shows mirror symmetry about the cell centerline. Figure 3b,e show the waves of torsion that propagate with the highly curved sections during the recovery stroke. Here, τ is plotted when it is well-defined, *i.e.* when $\kappa > 0.4\ \mu m^{-1}$ (an investigation of the effects of noise on τ is presented in the methods section and Fig. S1). The torsion in both CC-125 and CC-2288 has the opposite sign in cis and trans flagella at the start of the recovery stroke: the trans flagellum has predominantly negative torsion, while the cis flagellum has predominantly positive torsion. Figure 3c,f show the average torsion over approximately 600 beat cycles for the wildtype and mutant cell lines, during the recovery stroke only. The opposite polarity of the torsion can be seen most clearly in the wildtype (Fig. 3c), although the same trend is present and statistically significant in CC-2288. These subtle differences in the symmetries are likely to stem from inherent structural chirality (*e.g.*) dynein configuration), physical coupling to the basal body apparatus and hydrodynamic coupling to the cell body --- aspects that have been investigated in detail elsewhere (Vilfan and Jülicher 2006; Polin et al. 2009; Geyer et al. 2013; Brumley et al. 2014; Cheng et al. 2024). In contrast, at the initialisation of the power stroke, both flagella demonstrate a subtle rotational `shrugging' motion close to their bases (Fig. 3g,h,i, Supplementary Movie S1), reminiscent of the flagellar motion of the monoflagellate *Euglena* (Rossi et al. 2017). Both cis- and trans waveforms show the same chirality during this phase --- there is rotational symmetry about the cell's centerline. This is difference with the mirror-symmetry of the recovery stroke indicates that the patterns of dynein activation (Lin and Nicastro 2018) are critical to the chirality of the flagellar motion, which is not dictated by the structure alone.

Flagellar synchrony and beat coherence

The synchronization of multiple flagella on a single cell body is the subject of previous work focusing on organisms with one, two or many flagella (Brumley et al. 2012; Geyer et al. 2013; Brumley et al. 2014; Klindt et al. 2017). Discrete phase slips have been observed to resynchronize the beat of *C. reinhardtii* (Polin et al. 2019); we focus on the short time coherence of the flagellar beat --- how the beat frequency (and hence phase) fluctuates stochastically. Figure 4a shows $\kappa(t)$ for a section of a wildtype flagellum, at $s = 2\ \mu m$ from the cell body. The time series has been divided up into 0.6 second blocks and aligned so that the first peak in each series overlaps. The curvature is approximately periodic, but the frequency drifts enough to `smear out' the sinusoidal curvature for $t > 0.5$ seconds. To quantify this, we have plotted the autocorrelation of the curvature in the cis and trans flagella, κ_C and κ_T respectively, in Fig. 4b,c. The cross-correlation is shown in Fig. 4d. In all cases, the correlation functions take the form of a damped cosine function with characteristic

Journal of Cell Science • Accepted manuscript

decay time $t_c = 0.08$ sec, corresponding to 3–4 beat cycles. Figure 4e summarises t_c for all cells, showing no strong dependence on f.

Applying resistive force theory

Finally, we use our three-dimensional coordinates to apply a long-standing approximation of flagellar hydrodynamics: resistive force theory (RFT). This models the force (F) and torque (Γ) on the cell body due to the motion of its swimming apparatus. In RFT, a flagellum is modelled as locally straight, thin rod with drag coefficients that are different for motion tangential ($K_{\hat{t}}$) and normal ($K_{\hat{n}}$) to the rod axis. These coefficients were obtained theoretically by Lighthill (Lighthill 1976) in an analytical study of flagellar fluid dynamics, but experimental studies have found values that vary up to a factor of two from the theoretically-derived values (Bayly et al. 2011; Friedrich et al. 2010) and seem to depend somewhat on the experimental geometry and the species being studied. In our experimental setup the algal cell bodies cannot move freely, which prevents us from extracting values of the friction coefficients from the data; in the absence of this data, we impose the values obtained theoretically in the earlier work (explicitly, $K_{\hat{t}} = 1.85 \times 10^{-3}$ Pa·s, $K_{\hat{n}} = 3.22 \times 10^{-3}$ Pa·s). The net forces and torques on a freely swimming cell must equal zero in the absence of external constraints:

$$\mathrm{F_b} + \Sigma_\mathrm{i} \delta \mathrm{F_i} = 0$$

$$\Gamma_b + \Sigma_i (r_i \wedge \delta F_i) + \Sigma_i \delta \Gamma_i = 0$$

where the subscript b refers to the body, $\delta\Gamma_i$ is an element of torque caused by the rotation of a segment about its hydrodynamic centre, and δF_i is an element of force caused by the motion of a rod-like segment at position r_i relative to the hydrodynamic centre of the system. We present the net force and torque on the fluid due to the motion of the flagella in Figs. 4f,g., where the data points represent instantaneous measurements of force and the lines are guides to the eye obtained by fitting cubic smoothing splines to the data. In our experiments, the micropipette supplies an external force, and so the flow fields generated by the cell body and flagella will be qualitatively different to those produced by a freely-swimming individual.

To improve this approximation, we transform from the body-centred frame (indicated by primed quantities) in which we perform our imaging, to a notional lab frame in which the cell would swim freely. The hydrodynamic force δF experienced by a segment of the flagellum at position s and time

Journal of Cell Science • Accepted manuscript

t is resolved into components tangential and normal to the segment[1]. Hydrodynamic coupling with the cell body and between neighbouring segments is ignored. For a freely-swimming cell with velocity $\boldsymbol{v}_b$, the force experienced by a flagellar element moving with velocity $\boldsymbol{v}_i = \boldsymbol{v}_i' - \boldsymbol{v}_b$ in the lab frame is given by:

$$\delta \mathrm{F} = \mathrm{ds}\,[K_{\hat{t}}\left((v' - v_b)\cdot\hat{t}\right)\hat{t} + K_{\hat{n}}\left((v' - v_b)\cdot\hat{n}\right)\hat{n}\,].$$

The force and torque acting on the cell body are

$$F_b = 6\pi\eta a v_b$$

$$\Gamma_b = 8\pi\eta a^3 \boldsymbol{\Omega}_b,$$

where η is the dynamic viscosity of the medium, a is the cell body radius (obtained for each cell from the microscopy data), and $\boldsymbol{\Omega_b}$ is the angular velocity of the cell body. We approximate the cells as spheres for simplicity but one could but one could extend this to spheroids (Bayly et al. 2011).

By solving the equations for force and torque, we estimate the swimming speed and rotation frequency of free cells. These quantities, along with a measurement of flagellar beat frequency are plotted in Fig. 4(h–j), in which we compare the predictions produced by the RFT model to experimental data on freely-swimming cells with flagella of varying length (Khona et al. 2013; Bauer et al. 2021). We find that the swimming speed (Fig. 4h) is the quantity most strongly affected by the flagellar length. Rotational speed is largely independent of length in our measurements (Fig. 4i), and there is a weak trend towards decreasing beat frequency with increasing flagellar length (Fig. 4j), the latter in agreement with a previous study in a closely-related strain (Goldstein et al. 2011). The flagellar beat frequencies that we observe are at the lower end of those reported in previous studies, likely influenced by the relatively low temperature in our laboratory of 19 ± 0.5°C. *Chlamydomonas* swimming speed shows sensitivity to growth media and cell cycle time, but the swimming speeds inferred by the RFT model are within the range of previous measurements of the swimming dynamics in this species (Martinez et al. 2012; Khona et al. 2013; Fujita et al. 2014; Folcik et al. 2020; Bottier et al. 2019; Bauer et al. 2021; Cui et al. 2023); if the theoretically-derived friction coefficients are indeed overestimated, this would suggest that the resultant swimming speeds are overestimated for our flagellar beat frequencies. Although RFT is an appealing `first approximation' due to its simplicity, we caution that it does not capture the hydrodynamic interactions between the flagella, or between the flagella and cell body — see the work by Guasto *et al.*, (Guasto et al. 2010)

[1] To clarify, as we are modelling the flagellar element as a straight rod, the binormal direction is not defined. The `normal' component here refers to all non-tangential forces.

Journal of Cell Science • Accepted manuscript

for a quasi-two-dimensional study showing fluid flows. Theoretical studies have predicted that these longer-range hydrodynamic relationships play an important role in shaping the motion of molecular motors into a flagellar beat (Riedel-Kruse et al. 2007; Han and Peskin 2018; Cicuta 2020; Gaffney et al. 2021), and this should be taken into account in future analyses. Moreover, the presence of the pipette holding the cell body means that the fluid flows experienced by the flagella are different to those experienced by the flagella on a freely-swimming cell, and instead are closer to flows experienced by motile cilia attached to a sessile cell. Nevertheless, the analysis shows remarkable consistency with the observed swimming behavior (swimming speed and rotational speed), and this adds to our confidence in the measurements.

Discussion

We have obtained the first time-resolved, three-dimensional images of the flagellar beat of *Chlamydomonas reinhardtii*. In agreement with previous studies, we find that the beat planes of the cis and trans flagella are twisted with respect to each other, but our imaging approach carries significant additional advantages as we can measure chiral asymmetries in the flagellar waveform, and infer out-of-plane rotational dynamics that would not be captured by two-dimensional imaging. DHM allows instantaneous measurement of the flagellar contour with position resolution comparable to the flagellar diameter, and with no prior assumptions about the configuration or overall trajectory of the flagella. Our enhanced position information reveals curious asymmetries in the power and recovery stroke that are only revealed by high-speed three-dimensional imaging. Notably, the recovery stroke of the flagella shows a chiral asymmetry between cis and trans flagella, and the power stroke is initiated with a subtle rotational or `shrugging' motion reminiscent of the beat of the uniflagellate alga *Euglena*, or the chirality inversion in *Spiroplasma* bacteria (Shaevitz et al. 2005). Ultrastructural studies and experimental observations indicate that many eukaryotic flagella (including those of *Chlamydomonas*) possess an underlying bilateral symmetry owing to bridges between microtubule doublets in the axoneme (Dutcher 2019; Lindemann and Lesich 2021), or in connection with the axoneme's radial spokes or central pair of singlet microtubules (Poghosyan et al. 2020; Lindemann and Lesich 2024). Connecting this structural information to the function of flagella requires high-speed, three-dimensional imaging to capture the shape of the flagellar beat in detail, revealing changes caused by mutations in the flagellar machinery. Our imaging study shows a clear non-planar element present, especially near the base of the flagella at the initiation of the power stroke. Moreover, it shows the ability of flagella to invert the handedness of their waveform; for the tip to execute circular motion in a system with underlying bilateral symmetry shows the

Journal of Cell Science • Accepted manuscript

striking versatility of this organelle. Our data are consistent with that from previous two-dimensional imaging studies, and will help guide future studies by showing to what extent two-dimensional information is sufficient to answer some questions, especially around the synchronisation of the flagellar beat. In contrast, three-dimensional measurement of waveforms is likely to be necessary to establish how mutations in structural components affect beat regulation, particularly in the basal region of the flagellum at the initiation of the power stroke. More broadly, in combination with genetic manipulations our technique will enable studies to give deeper insight into the mechanical role of various flagellar components, and accelerate the development and testing of robotic microswimmers inspired by biological systems.

Methods

Our study makes extensive use of inline digital holographic microscopy (DHM) to image flagella in three dimensions, and at relatively high frame rates (800\,Hz). We outline the main stages of the image acquisition and processing, as well as cell culture conditions, below.

Optical setup

A Nikon Eclipse Ti microscope was fitted with a custom-built swinging `arm' that allowed the illumination mode to be switched easily between dark field imaging and DHM while holding a cell on a micropipette. Dark field imaging was performed using a 10× magnification lens to locate and trap cells, before a 60× oil immersion lens was gently moved into position to perform DHM imaging. We implemented DHM using a fiber-coupled laser diode (wavelength λ=642 nm) in an inverted microscope as described previously (Giuliano et al. 2014; Kuhn et al. 2018). Holograms were obtained using a 60× oil-immersion objective lens (NA 1.45) and a Mikrotron MC-1362 camera, resulting in an effective pixel size of 0.233µm. Three videos of 10,000 frames each were acquired from each cell (N=20 cells for WT strain CC-125 and N=16 cells for strain CC-2288) at a frame rate of 800 Hz, and an exposure time of 800 µs. The cells were held approximately 10 µm from the focal plane in order to avoid complications arising from the holographic `twin-image problem' in which the real and virtual image reconstructions are found in close proximity (Kim 2010). The microscope stage was defocused slightly between each movie capture on the same cell, to allow a range of sample depths for reconstruction. Sample chambers measuring 10 mm × 10mm × 1 mm were constructed from glass slides and UV-curing glue, allowing a large enough aperture to accommodate

Journal of Cell Science • Accepted manuscript

a glass micropipette. Micropipettes were fabricated with an outer tip diameter of around 10 μm and an inner diameter of around 2 μm, as pictured in Fig 1 of the main manuscript.

Image analysis

We used a Kalman filter to improve the signal-to-noise ratio in our movies by removing slow-moving features, and hand-drawn masks to isolate the regions in which the flagella move. The movies were analysed using Rayleigh-Sommerfeld back propagation (Lee and Grier 2007) combined with a Sobel-type filter to localise the flagella in three dimensions (Wilson and Zhang 2012). The flagellar contours were refined as in previous work (Wilson et al. 2013), which we briefly recap here. Nodes along the flagellar contour were identified by stepping through the point cloud data at intervals of 0.7 μm . The contours began with the base of the flagellum, the position of which was identified from the raw data by eye in each case. The contours were smoothed using a piecewise cubic spline. The smoothed spline was resampled to ensure a constant value for contour length between each (resampled) node, in each frame. For the purposes of computing the curvature and torsion, the flagella were approximated to be locally straight between nodes. Camera noise occasionally resulted in a flagellum appearing truncated. In these cases, the flagellar location was interpolated between neighbouring frames; this approach was not used in cases where the apparent truncation was systematic and due to (*e.g.*) inconvenient placement of the cell body. Additional details about the calculation of curvature, torsion, and their associated uncertainties are given in the following section. To obtain a cycle-averaged movie of the flagellar beat, the curvature of the flagellum at $s = 2$ µm was plotted, and divided into `blocks' of around 0.5 seconds. The first peak in each block was used to align the blocks in time to obtain cycle-averaged flagellar motion, shown in the movie in the Supporting Information.

Uncertainties in force, torque, curvature and torsion

Using digital holographic microscopy (DHM), the uncertainties in locating the flagellar centreline in the x, y plane are similar to those in bright field microscopy -- conservatively, half a pixel, equivalent to $\sim$ 100 nm in our case. The axial uncertainty is around 1.5 $\times$ larger (Wilson and Zhang 2012), due to the finite numerical aperture of the imaging system. To estimate the uncertainties in $\boldsymbol{F}, \boldsymbol{\Gamma}, \kappa$ and τ, we performed Monte Carlo simulations based on the averaged flagellar beat cycle as depicted in Figs. 1c,d in the main manuscript. Each `frame' from this averaged representation was equivalent to 0.004 sec, or 1/50th of a beat cycle. We re-sampled the contour $P(r, t)$ from 0.4 µm (the value used for analysis) to 0.7 µm between nodes (0.7 µm was the value used in the initial DHM imaging) using

Journal of Cell Science • Accepted manuscript

spline interpolation in three dimensions to obtain an estimate of the noise-free contour, $P(r,t)$. We then added Gaussian noise to this data (mean value of zero, standard deviation of 100 nm) to give a new contour $P_n(r,t)$, and recalculated values for the derived quantities, repeating the measurements around one hundred times to better capture the standard deviation of the uncertainties. These uncertainties were on the order of 0.3 pN for the force, and 1 pN$\cdot$nm for torque (cf. Fig. 4f,g in the main text). Next, we estimated curvature and torsion in the presence of simulated noise (κ_n and τ_n respectively) via our standard analysis scheme. The standard deviation of (τ_n - τ) is shown in Supplementary Fig. 1, where each data point represents a set of 100 realisations of τ_n. We imposed an additional `cut-off' variable so that values of τ are discarded if κ at the same location is less than a certain threshold, denoted on the horizontal axis. As this criterion is made stricter (*i.e.* as the κ cut-off is raised), fewer values for τ are considered, and the standard deviation falls as only the better-defined values are retained. We have chosen a cut-off value for $\kappa > 0.4\ \mu m^{-1}$ for our main analysis, corresponding to the unshaded region in Supplementary Fig. 1. The standard deviation of ($\kappa_n - \kappa$) is approximately $\mathcal{O}(0.1)\ \mu m^{-1}$, small compared to the values of curvature recorded in Fig. 3a,d.

Cell culture

Algal strains were obtained from the *Chlamydomonas* Resource Center at the University of Minnesota. The cells were grown in tris-acetate-phosphate (TAP) medium to a density of around 10^5 cells/ml, under a 12-hour light-dark cycle. Cells were harvested by gentle aspiration into a pipette, and loaded into the sample chambers described above. The micropipette was then introduced to the sample volume, and were cells captured individually for imaging.

Acknowledgements

We thank B. Friedrich for technical suggestions, and A.M. Phillips for helpful discussions.

Competing Interests

No competing interests declared.

Contribution

L.G.W. designed and performed research; L.G.W. and M.A.B. analysed data and wrote the paper.

Journal of Cell Science • Accepted manuscript

Funding

This work was supported by EPSRC grant EP/N014731/1 (LW) and Royal Society Exchange Grant IEC/R3/183084 (MB).

Data availability

Underlying data are available at https://doi.org/10.15124/d4e84b6b-af05-4b77-9ca1-dc695f1160e9

References

D. Bauer, H. Ishikawa, K.A. Wemmer, N.L. Hendel, J. Kondev, and W.F. Marshall. Analysis of biological noise in the flagellar length control system. *iScience*, 24:102354, 2021.

P.V. Bayly, B.L. Lewis, E.C. Ranz, R.J. Okamoto, R.B. Pless, and S.K. Dutcher. Propulsive forces on the flagellum during locomotion of *Chlamydomonas reinhardtii*. *Biophys. J.*, 100(11):2716–2725, 2011.

S. Bianchi, F. Saglimbeni, and R. Di Leonardo. Holographic imaging reveals the mechanism of wall entrapment in swimming bacteria. *Phys. Rev. X*, 7:011010, 2017.

M. Bottier, K.A. Thomas, S.K. Dutcher, and P.V. Bayly. How does cilium length affect beating? *Biophys. J.*, 116:1292–1304, 2019.

J.J. Breunig, J.I. Arellano, and P. Rakic. Cilia in the brain: going with the flow. *Nat. Neurosci.*, 13(6):654–655, 2010.

D.R. Brumley, M. Polin, T.J. Pedley, and R.E. Goldstein. Hydrodynamic synchronization and metachronal waves on the surface of the colonial alga *Volvox carteri*. *Phys. Rev. Lett.*, 109:268102, 2012.

D.R. Brumley, K.Y. Wan, M. Polin, and R.E. Goldstein. Flagellar synchronization through direct hydrodynamic interactions. *eLife*, 3:e02750, 2014.

K.H. Bui, T. Yagi, R. Yamamoto, R. Kamiya, and T. Ishikawa. Polarity and asymmetry in the arrangement of dynein and related structures in the *Chlamydomonas* axoneme. *J. Cell. Biol.*, 198(5):913–925, 2012.

A. Bukatin, I. Kukhtevich, N. Stoop, J. Dunkel, and V. Kantsler. Bimodal rheotactic behavior reflects flagellar beat asymmetry in human sperm cells. *Proc. Natl. Acad. Sci. USA*, 112:15904–15909, 2015.

Journal of Cell Science • Accepted manuscript

Z. Cheng, A. Vilfan, Y.Wang, R. Golestanian, and F. Meng. Near-field hydrodynamic interactions determine travelling wave directions of collectively beating cilia. *J. Roy. Soc. Interface*, 21:20240221, 2024.

F. C. Cheong, C. C. Wong, Y. F. Gao, M. H. Nai, Y. Cui, S. Park, L. J. Kenney, and C. T. Lim. Rapid, high-throughput tracking of bacterial motility in 3d via phase-contrast holographic video microscopy. *Biophys. J.*, 108:1248–1256, 2016.

P. Cicuta. The use of biophysical approaches to understand ciliary beating. *Biochem Soc. Trans.*, 48:221–229, 2020.

D. Cortese and K.Y. Wan. Control of helical navigation by three-dimensional flagellar beating. *Phys. Rev. Lett.*, 126:088003, 2021.

M. Cui, S.K. Dutcher, P.V. Bayly, and J.M Meacham. Robust acoustic trapping and perturbation of single-cell microswimmers illuminate three-dimensional swimming and ciliary coordination. *Proc. Natl. Acad. Sci. USA*, 120(25):e2218951120, 2023.

S.K. Dutcher. Asymmetries in the cilia of *Chlamydomonas*. *Phil. Trans. Roy. Soc. B*, 375:20190153, 2019.

R. Findlay, M. Osman, K.A. Spence, P.M. Kaye, P.B. Walrad, and L.G. Wilson. High-speed, three-dimensional imaging reveals chemotactic behaviour specific to human-infective *Leishmania* parasites. *eLife*, 10:65051, 2021.

A.M. Folcik, T. Haire, K. Cutshaw, M. Riddle, C. Shola, S. Nassani, P. Rice, B. Richardson, P. Shah, N. Nazamoddini-Kachouie, and A. Palmer. Computer-assisted tracking of *Chlamydomonas* species. *Front. Plant Sci.*, 10:1616, 2020.

B.M. Friedrich, I.H. Riedel-Kruse, J. Howard, and F. Julicher. High-precision tracking of sperm swimming fine structure provides strong test of resistive force theory. *J. Expt. Biol.*, 213:1226–1234, 2010.

S. Fujita, T. Masao, M. Ishiura, and M. Kikkawa. High-throughput phenotyping of *Chlamydomonas* swimming mutants based on nanoscale video analysis. *Biophys. J.*, 107:336–345, 2014.

E.A. Gaffney, H. Gadelha, D.J. Smith, J.R. Blake, and J.C. Kirkman-Brown. Mammalian sperm motility: Observation and theory. *Ann. Rev. Fluid Mech.*, 43:501–528, 2011.

E.A. Gaffney, K. Ishimoto, and B.J. Walker. Modelling motility: The mathematics of spermatozoa. *Front. Cell Dev. Biol.*, 9:710825, 2021.

Journal of Cell Science • Accepted manuscript

V.F. Geyer, F. Julicher, J. Howard, and B.M. Friedrich. Cell-body rocking is a dominant mechanism for flagellar synchronization in a swimming alga. *Proc. Natl. Acad. Sci. USA*, 110(45):18058–18063, 2013.

T. Gibson, M. Bedrossian, E. Serabyn, C. Lindensmith, and J.L. Nadeau. Using the gouy phase anomaly to localize and track bacteria in digital holographic microscopy 4d images. *J. Opt. Soc. Am. A*, 38(2):A11–A18, 2021.

C. B. Giuliano, R. Zhang, and L. G. Wilson. Digital inline holographic microscopy (dihm) of weakly-scattering subjects. *J. Vis. Exp.*, 84:e50488, 2014.

R.E. Goldstein, M. Polin, and I. Tuval. Emergence of synchronized beating during the regrowth of eukaryotic flagella. *Phys. Rev. Lett.*, 107:148103,2011.

A. Gong, S. Rode, G. Gompper, U.B. Kaupp, J. Elgeti, B.M. Friedrich, and L. Alvarez. Reconstruction of the three-dimensional beat pattern underlying swimming behaviors of sperm. *Eur. Phys. J. E*, 44:87, 2021.

J.S. Guasto, K.A. Johnson, and J.P. Gollub. Oscillatory flows induced by microorganisms swimming in two dimensions. *Phys. Rev. Lett.*, 105(16): 168102, 2010.

J. Han and C.S. Peskin. Spontaneous oscillation and fluid-structure interaction of cilia. *Proc. Natl. Acad. Sci. USA*, 115(17):4417–4422, 2018.

M.D. Hannel, A. Abdulali, M. O'Brien, and D.G. Grier. Machine-learning techniques for fast and accurate feature localization in holograms of colloidal particles. *Opt. Express*, 26(12):15221–15231, Jun 2018.

N. Hirokawa, Y. Okada, and Y. Tanaka. Fluid dynamic mechanism responsible for breaking the left-right symmetry of the human body: The nodal flow. *Ann. Rev. Fluid Mech.*, 41:53–72, 2009.

H.J. Hoops and G.B. Witman. Outer doublet related to beat heterogeneity reveals structural polarity direction in *Chlamydomonas* flagella. *J. Cell Biol.*, 97:902–908, 1983.

H.J. Hoops, R.L. Wright, J.W. Jarvik, and G.B. Witman. Flagellar waveform and rotational orientation in a *Chlamydomonas* mutant lacking normal striated fibers. *J. Cell. Biol.*, 98:818–824, 1984.

I. Inouye and T. Hori. High-speed video analysis of the flagellar beat and swimming patterns of algae: possible evolutionary trends in green algae. *Protoplasma*, 164:54–69, 1991.

J. F. Jikeli, L. Alvarez, B. M. Friedrich, L. G. Wilson, R. Pascal, R. Colin, M. Pichlo, A. Rennhack, C. Brenker, and U. B. Kaupp. Sperm navigation along helical paths in 3d chemoattractant landscapes. *Nat. Commun.*, 6:7985, 2015.

Journal of Cell Science • Accepted manuscript

A.V. Kanale, F. Ling, H. Guo, S. Furthauer, and E. Kanso. Spontaneous phase coordination and fluid pumping in model ciliary carpets. *Proc. Natl. Acad. Sci. USA*, 119(45):e214413119, 2022.

S. Khan and J.M. Scholey. Assembly, functions and evolution of archaella, flagella and cilia. *Curr. Biol.*, 28:R278–R292, 2018.

D.K. Khona, V.G. Rao, M.J. Motiwalla, P.C.S. Varma, A.R. Kashyap, K. Das, S.M. Shirolikar, L. Borde, J.A. Dharmadhikari, A.K. Dharmadhikari, S. Mukhopadhyay, D. Mathur, and J.S. D'Souza. Anomalies in the motion dynamics of long-flagella mutants of *Chlamydomonas reinhardtii*. *J. Biol. Phys.*, 39:1–14, 2013.

M.K. Kim. Principles and techniques of digital holographic microscopy. *SPIE Rev.*, 1:018005, 2010.

G.S. Klindt, C. Ruloff, C. Wagner, and B.M. Friedrich. In-phase and antiphase flagellar synchronization by waveform compliance and basal coupling. *New. J. Phys.*, 19:113052, 2017.

M.J. Kuhn, F.K. Schmidt, N.E. Farthing, F.M. Rossmann, B. Helm, L.G. Wilson, B. Eckhardt, and K.M. Thormann. Spatial arrangement of several flagellins within bacterial flagella improves motility in different environments. *Nat. Commun.*, 9:5369, 2018.

S.-H. Lee and D. G. Grier. Holographic microscopy of holographically trapped three-dimensional structures. *Opt. Express*, 15(4):1505–1512, 2007.

J. Lighthill. Flagellar hydrodynamics. *SIAM Review*, 18(2):161 – 230, 1976.

J. Lin and D. Nicastro. Asymmetric distribution and spatial switching of dynein activity generates ciliary motility. *Science*, 360(6387):eaar1968, 2018.

C.B. Lindemann and K.A Lesich. The many modes of flagellar and ciliary beating: Insights from a physical analysis. *Cytoskeleton*, 78:36–51, 2021.

C.B. Lindemann and K.A Lesich. The mechanics of cilia and flagella: What we know and what we need to know. *Cytoskeleton*, 81:648--668, 2024.

V.A. Martinez, R. Besseling, O.A. Croze, J. Tailleur, M. Reufer, J. Schwarz-Linek, L.G. Wilson, M.A. Bees, and W.C.K. Poon. Differential dynamic microscopy: A high-throughput method for characterizing the motility of microorganisms. *Biophys. J.*, 103:1637–1647, 2012.

S.A. Matthews, C. Coelho, E.E. Rodriguez Salas, E.E. Brock, V.J. Hodge, J.A. Walker, and L.G. Wilson. Real-time 3d tracking of swimming microbes using digital holographic microscopy and deep learning. *PLoS One*, 19:e0301182, 04 2024.

Journal of Cell Science • Accepted manuscript

S. Mojiri, S. Isbaner, S. Muhle, H. Jang, A.J. Bae, I. Gregor, A. Gholami, and J. Enderlein. Rapid multi-plane phase-contrast microscopy reveals torsional dynamics in flagellar motion. *Biomed. Opt. Express*, 12(6):3169–3180, 2021.

M. Molaei, M. Barry, R. Stocker, and J. Sheng. Failed escape: Solid surfaces prevent tumbling of *Escherchia coli*. *Phys. Rev. Lett.*, 113:068103, 2014.

D. Nicastro, C. Schwartz, J. Pierson, R. Gaudette, M.E. Porter, and J.R. McIntosh. The molecular architecture of axonemes revealed by cryoelectron tomography. *Science*, 313(5789):944–948, 2006.

T. Oda, H. Yanagisawa, R. Kamiya, and M. Kikkawa. A molecular ruler determines the repeat length in eukaryotic cilia and flagella. *Science*, 346(6211):857–860, 2014.

M. Owa, T. Uchihashi, H.-A. Yanagisawa, T. Yamano, H. Iguchi, H. Fukuzawa, K.-I.Wakabayashi, and T. Ando M. Kikkawa. Inner lumen proteins stabilize doublet microtubules in cilia and flagella. *Nat. Commun.*, 10:1143, 2019.

E. Poghosyan, I. Iacovache, L. Faltova, A. Leitner, P. Yang, D.R. Diener, R. Aebersold, B. Zuber, and T. Ishikawa. The structure and symmetry of the radial spoke protein complex in *Chlamydomonas* flagella. *Phil. Trans. Roy. Soc. B*, 133(16):jcs245233, 2020.

M. Polin, I. Tuval, K. Drescher, J.P. Gollub, and R.E. Goldstein. *Chlamydomonas* swims with two "gears" in a eukaryotic version of run-and-tumble locomotion. *Science*, 325:487–490, 2009.

I.H. Riedel-Kruse, A. Hilfinger, J. Howard, and F. Julicher. How molecular motors shape the flagellar beat. *HFSP J.*, 1(3):192–208, 2007.

M. Rossi, G. Cicconofri, A. Beran, G. Noselli, and A. DeSimone. Kinematics of flagellar swimming in *Euglena gracilis*: Helical trajectories and flagellar shapes. *Proc. Natl. Acad. Sci USA*, 114(50):13085–13090, 2017.

U. Rüffer and W. Nultsch. High-speed cinematographic analysis of the movement of *Chlamydomonas*. *Cell Motility*, 5:251–263, 1985.

U. Rüffer and W. Nultsch. Flagellar photoresponses of *Chlamydomonas* cells held on micropipettes: I. change in flagellar beat frequency. *Cell Mot. Cytoskel.*, 15:162–167, 1990.

U. Rüffer and W. Nultsch. Flagellar photoresponses of *Chlamydomonas* cells held on micropipettes: Ii. change in flagellar beat pattern. *Cell Mot. Cytoskel.*, 18:269–278, 1991.

J.W. Shaevitz, J.Y. Lee, and D.A. Fletcher. *Spiroplasma* swim by a processive change in body helicity. *Cell*, 122:941–945, 2005.

Journal of Cell Science • Accepted manuscript

J. Sheng, E. Malkiel, J. Katz, J. Adolf, R. Belas, and A. R. Place. Digital holographic microscopy reveals prey-induced changes in swimming behavior of predatory dinoflagellates. *Proc. Natl. Acad. Sci. USA*, 104:17512–17517, 2007.

M. Striegler, B.M. Friedrich, S. Diaz, and V.F. Geyer. Twist - torsion coupling in beating axonemes. *Nat. Phys.*, 21:599-607, 2025.

T.W. Su, L. Xue, and A. Ozcan. High-throughput lensfree 3d tracking of human sperms reveals rare statistics of helical trajectories. *Proc. Natl. Acad. Sci. USA*, 109:16018–16022, 2012.

K.L. Thornton, J.K. Butler, S.J. Davis, B.K. Baxter, and L.G. Wilson. Haloarchaea swim slowly for optimal chemotactic efficiency in low nutrient environments. *Nat. Commun.*, 11:4453, 2020.

A. Vilfan and F. Julicher. Hydrodynamic flow patterns and synchronization of beating cilia. *Phys. Rev. Lett.*, 96:058102, 2006.

L. G. Wilson, L. M. Carter, and S. E. Reece. High-speed holographic microscopy of malaria parasites reveals ambidextrous flagellar waveforms. *Proc. Natl. Acad. Sci. USA*, 110(47):18769-18774, 2013.

L. Wilson and R. Zhang. 3d localization of weak scatterers in digital holographic microscopy using Rayleigh-Sommerfeld backpropagation. *Opt. Express*, 20(15):16735-16744, 2012.

Journal of Cell Science • Accepted manuscript

Figures

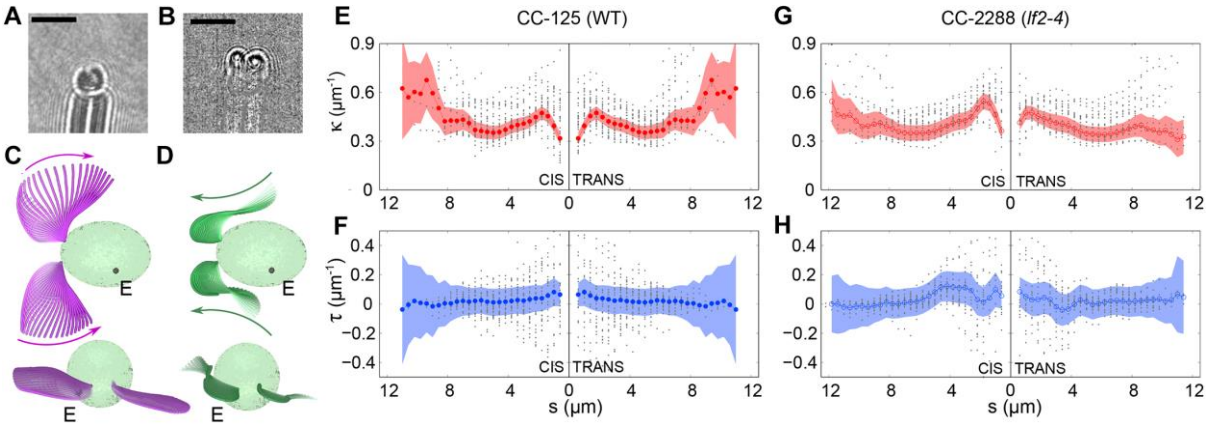

Fig. 1. (a) Raw holographic data showing a cell on a micropipette, approximately 5 μm below the focal plane (scale bar shows 10 μm). (b) Holographic data after background subtraction, showing the flagella. (c),(d) Rendering of the cell body and flagella during power and recovery stroke, respectively; **E** indicates the cell's eye spot. (e),(f), Mean curvature and torsion of the cis and trans flagella, for the wildtype strain CC-125. Grey data points correspond to values from individual movies, and the shaded areas indicate a 95% CI. (g),(h) Mean curvature and torsion values for the mutant strain CC-2288.

Journal of Cell Science • Accepted manuscript

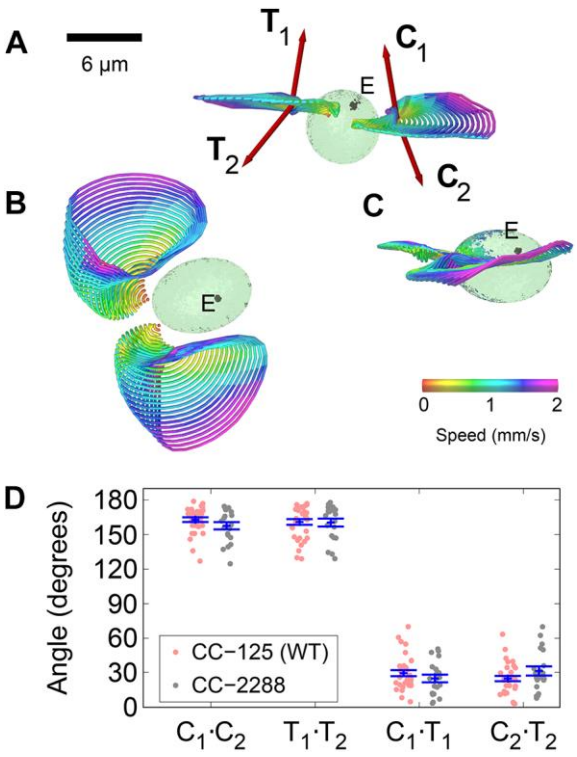

Fig. 2. (a) Beat plane normal vectors for power and recovery stroke of *C. reinhardtii* CC-125, for the cis ($C_{1,2}$) and trans ($T_{1,2}$) flagella. **E** indicates the eye-spot. (b),(c) Top and side views of the beat planes. (d) Angles between power and recovery strokes for strains CC-125 and CC-2288. Blue data points represent the mean angles; the error bars on these represent standard error on the mean.

Journal of Cell Science • Accepted manuscript

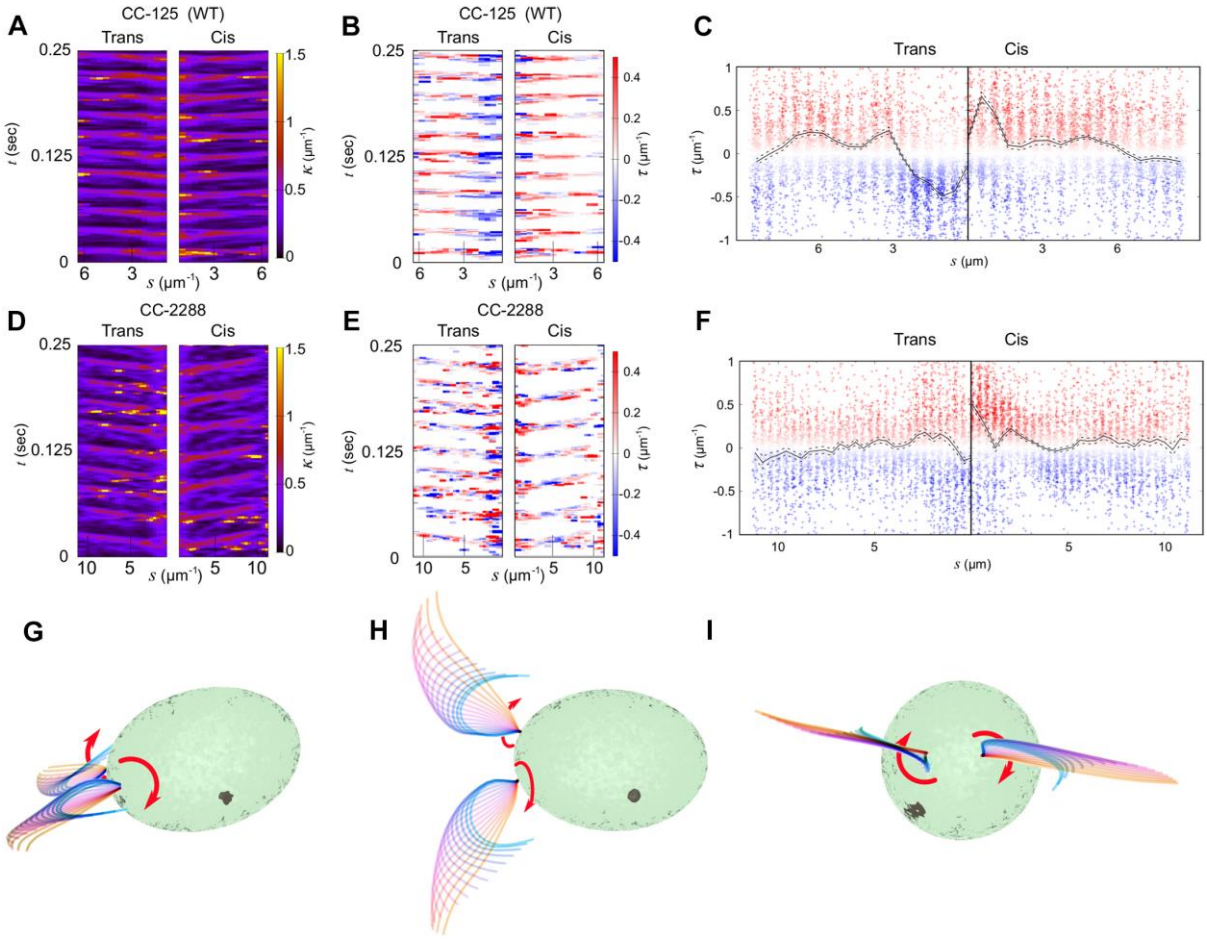

Fig. 3. (a) Kymograph showing $\kappa(t)$ for wildtype strain CC-125. Waves initiate at the base ($s = 0$) and propagate to the tip in both cis and trans flagella. (b) Torsion during the highest-curvature part of the beat cycle. Negative torsion is predominant in the trans flagellum (blue colors) and positive torsion in the cis flagellum (red colors) near $s = 0$. (c) Average (black lines) and instantaneous (points) torsion during 600 recovery strokes (12 seconds), showing $\tau < 0$ ($\tau > 0$) torsion in the proximal region of the trans (cis) flagellum. Dashed lines represent standard error on the mean. (d),(e),(f) Curvature and torsion in the strain CC-2288. The same qualitative trend in torsion around the $s = 0$ obtains, with a smaller magnitude. (g),(h),(i) Side, top and head-on projections showing the quasi-rotational `shrugging' motion occurring at the proximal end of the flagella, at the onset of the power stroke. The flagella are drawn with a radius of 50 nm to clarify the motion (approximately half the true value), and the red arrows show the direction of rotation.

Journal of Cell Science • Accepted manuscript

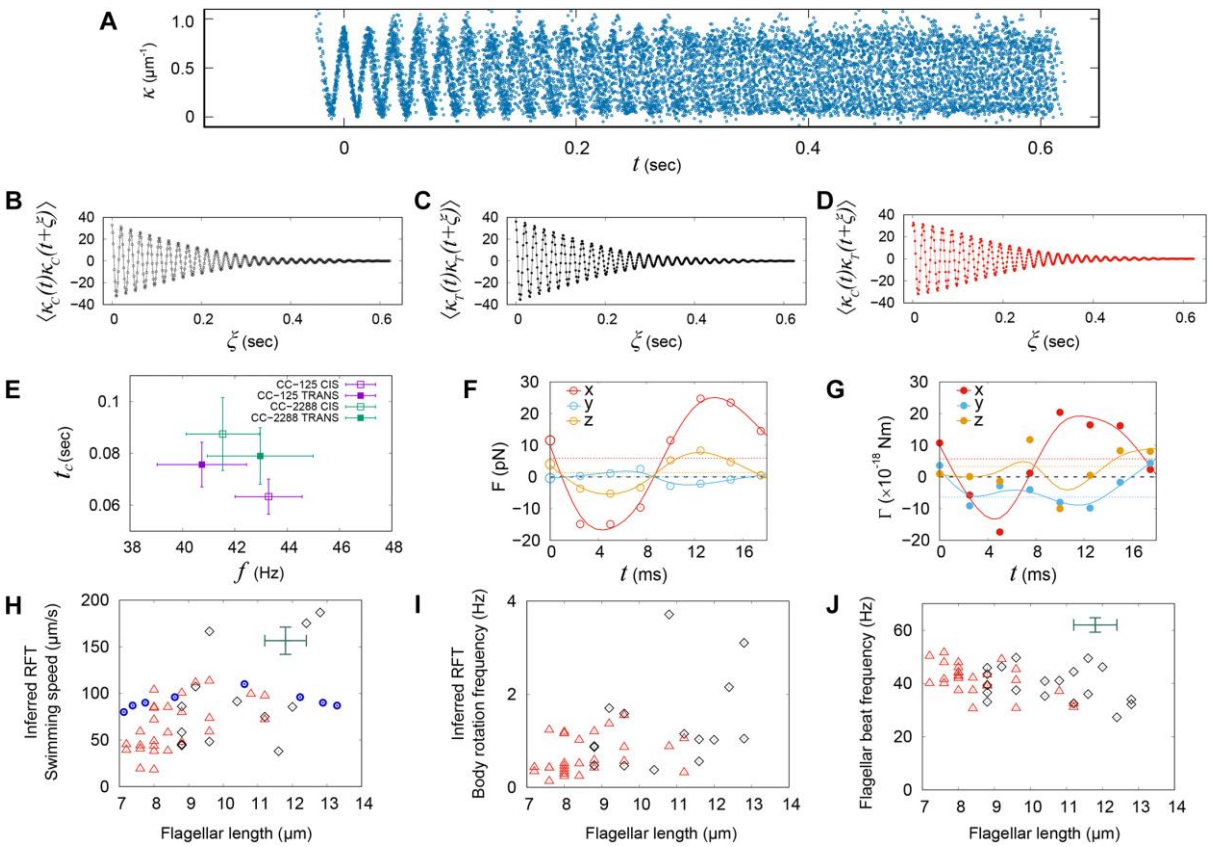

Fig. 4. (a) Aligned blocks of 0.6 seconds of curvature data at $s = 2$ μm in CC-125. Waves of curvature lose coherence at approximately 0.6 seconds. (b),(c) Autocorrelation of curvature in the cis and trans flagella (respectively) at $s = 2$ μm, as a function of delay time ξ. (d) Cross-correlation of curvature in cis and trans flagellum from a cell of strain CC-125. Decorrelation occurs slightly faster than in panels (b), (c) due to occasional periods of asymmetric flagellar beating. (e) Beat coherence time t_c as a function of average beat frequency f in the cis and trans flagella of strains CC-125 and CC-2288. Error bars denote standard error on the mean. (f) Instantaneous force on the fluid due to the beating action of the flagella, across an averaged beat cycle of a representative cell. The x-direction is defined by a line connecting the cell body centre-of-mass to a point halfway between the bases of the flagella; the y direction lies in the image plane (roughly in the plane of the flagellar beat), and the z-axis completes the right-handed coordinate system. Uncertainties on this averaged data are smaller than the data points (see methods). The black dashed line indicates zero force, and the colored dashed lines indicate the cycle-averaged force in each direction. (g) Instantaneous torque on the fluid due to the beating action of the flagella,

Journal of Cell Science • Accepted manuscript

across an averaged beat cycle of a representative cell, using the same coordinate system as panel (f). Uncertainties on this averaged data are smaller than the data points. The black dashed line indicates zero torque, and the colored dashed lines indicate the cycle-averaged torque in each direction. (h) Predicted swimming speed obtained from RFT, based on the motion of flagellar segments. Each point represents one cell of wildtype strain CC-125 (red triangles) or `long flagella' mutant CC-2288 (black diamonds). The green cross and blue points represent comparable literature data from references (Khona et al. 2013) and (Bauer et al. 2021), respectively. (i) RFT prediction of cell body rotation speed. Red and black points indicate strains CC-125 and CC-2288 as in panel (h). (j) Average flagellar beat frequency obtained from a Fourier analysis of flagellar curvature, $\kappa(t)$. Red and black points indicate strains CC-125 and CC-2288 as in panel (h); the green cross indicates literature data from ref. (Khona et al. 2013).

Journal of Cell Science • Accepted manuscript

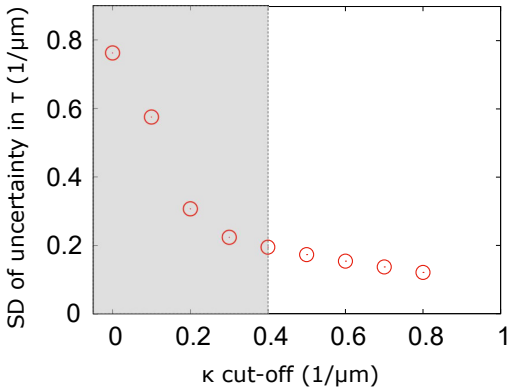

Fig. S1. Analysis of uncertainties in τ. Gaussian noise was added to the averaged flagellar coordinates presented in Figs. 1c,d of the main text, and the values for torsion recalculated. This figure shows the standard deviation of the errors incurred by the addition of noise. We retain the most robust values for torsion by discarding those values where κ lies in the shaded region of this figure. The values retained are the ones presented in Figs. 3b,e of the main text. Each data point represents the average of 100 realisations of the Monte Carlo simulations, for which the standard error on the mean for each data point is smaller than 10^{-4} $\mu\mathrm{m}^{-1}$ and therefore much smaller than the plotted points.

Dataset 1. The data here represent the frames of the supplementary movie of beating flagella of a cell of *Chlamydomonas reinhardtii* CC-125, with cis- and trans-associations indicated in the file names. Columns 1,2,3 represent x,y and z respectively, in micrometres. The data are arranged into blocks of 20 data points (flagellar segments). Each block corresponds to a single averaged time instance, with each beat divided into 50 'frames' (each approximately 400 microseconds in duration).

Available for download at
https://journals.biologists.com/jcs/article-lookup/doi/10.1242/jcs.263946#supplementary-data

Journal of Cell Science • Supplementary information

Movie 1. '3D rendering of a *C. reinhardtii* cell obtained by digitalholographic microscopy'

The move shows a 3D rendering of the *C. reinhardtii* flagellar beat obtained by holographic microscopy. The cell body measures around 8 μm in diameter, and the flagella have a radius of 110 nm. At the default frame rate of 25 frames per second, the movie is replayed at 1/100th of the true speed. The dark sphere represents the location of the eye spot.

Journal of Cell Science • Supplementary information